J. Fluid Mech. (2000), *vol.* 410, *pp.* 101–122. Printed in the United Kingdom

Low Reynolds number two-dimensional separated and reattaching turbulent shear flow

By P. E. HANCOCK

School of Mechanical and Materials Engineering, University of Surrey, Guildford, Surrey GU2 5XH, UK

(Received 25 January 1999 and in revised form 16 December 1999)

Pulsed-wire measurements of the streamwise mean velocity and Reynolds stress, mean and fluctuating surface shear stress, and other statistics have been made in a sharp-edged turbulent separation bubble formed behind a normal flat plate mounted on the front of a long splitter plate, covering nearly a decade range of low Reynolds number. The streamwise Reynolds stress increases appreciably with Reynolds number, from a level comparable with that in an isolated plane mixing layer to more than twice that level, while the change in the mean flow is at most slight. It is inferred using previous measurements that the other stresses do not change as much, thereby leaving the mean flow relatively unaffected. The mean wall shear stress and the r.m.s. of the (streamwise) fluctuations decrease in fixed proportion with increasing Reynolds number. Normalized p.d.f. distributions of velocity and wall shear stress do not change, except in the vicinity of the secondary separation bubble. At low Reynolds number the development length of the overlying mixing layer is an appreciable proportion of the bubble length, the development length being a function of the momentum thickness at separation. It is argued that the observed changes with Reynolds number in the bulk of the flow arise primarily as a result of a change in response of this layer to the fluctuating rates of strain imposed by the recirculating flow; at a low Reynolds number the response of the shear layer structures to the fluctuating rates of strain is less than it is at a high Reynolds number. As a consequence of the sensitivity to fluctuating strain rates the structure of the layer differs fundamentally from that of an isolated mixing layer.

The measurements help to reconcile previous measurements in this flow geometry which otherwise appear to be inconsistent. Moreover, in most of the previous measurements the flow width was not sufficient for end effects to have been negligible, most noticeably in the near-wall flow, where such effects are largest.

1. Introduction

Numerous experimental studies of nominally two-dimensional turbulent separated flow have been made, the most popular simple geometry being the backward-facing step. Imposing two-dimensionality is of course intended to reduce the degree of complexity without losing essential features of the separated and reattaching flow. The central region of such flows should therefore be free of any significant effects of the flows in the adjacent 'side' or 'end' regions. However, it is a matter of experiment as to how wide the flow should be in order for these end effects to be insignificant in all key respects, and it is clear that some features are more easily influenced

	$U_r h_f/\nu \times 10^3$	h_f/D	W/h_f	X_A/h_f	W/X_A	Side plates
Ruderich & Fernholz (RF)	14	0.09	23	17.2	1.3	No
Castro & Haque (CH)	11	0.06	19	19.2	1.0	Yes
Jaroch & Fernholz (JF)	14	0.022	63	25.0	2.5	No
Hancock & McCluskey (HM)	1.6	0.008	174	26.4	6.4	No
Hancock & Castro (HC)	1.8	0.014	20–80	25.3	0.8–3.2	Yes
Hancock (1999)	1–3.4	0.008	165	28.9	5.7	No
Present large fence	15	0.022	63	25.9	2.5	No
Present small fence	2–13	0.011	127	31.7	4.0	No

TABLE 1. Parameters for the various flow measurements discussed. Note that in this table the reference velocity, U_r, is as defined in the various studies, and not as redefined here.

than others. End effects can be avoided by using axisymmetric flows, though such arrangements have some not insignificant practical drawbacks. Of course, an implicit assumption for either planar or axisymmetric flows is that two-dimensional mean flow is indeed possible. Other than some random organisation the only alternative is a periodic cellular structure, though there is no evidence for such a structure in the present type of flow.

The measurements in the study here have been made in the separation bubble behind a flat plate normal to the oncoming flow, and mounted symmetrically at the front of a 'splitter' plate. Detailed measurements of the turbulence structure in this type of flow have been made by Ruderich & Fernholz (1986), Castro & Haque (1987), Jaroch & Fernholz (1989) and Hancock & McCluskey (1997), hereafter abbreviated as RF, CH, JF and HM, respectively. Salient parameters are given in table 1, where X_A is the distance to attachment, W is the flow width, and D is the half-height of the wind tunnel. In the terminology of Bradshaw & Wong (1972) the present type of flow is an 'overwhelming' perturbation.

In the first two cases of table 1 the flow width was about one bubble length, and it is clear, particularly from the first, that the influence of the side regions was significant in several respects, one example being the surface streamlines. The experiments by JF were therefore made in a wider flow, of about 2.5 bubble lengths, though they found the flow to be still significantly influenced by the side regions. Moreover, the levels of all the Reynolds stresses were much higher than had been measured in the previous studies, by a factor of roughly two or more, from which they inferred that a larger flow width would lead to still higher levels of Reynolds stress, before end effects ceased. In contrast, the measurements of HM in a flow which was six bubble lengths in width gave Reynolds stress levels near attachment that were about half those measured by RF. All of these measurements were made using broadly identical pulsed-wire techniques at the Universities of Berlin and Surrey. Despite these large differences the mean flow features show little variation (e.g. figure 2*a*). Taking account of the fact that the mean flow is dependent on gradients of the Reynolds stresses, such large differences in the stresses contradict the near constancy in the mean flow, unless the differences in the stress gradients are such as to have only a relatively small *net* effect on the mean momentum. The purpose of the measurements reported here was to reconcile the measurements of RF, JF, CH, HM and also Hancock & Castro (1993), hereafter denoted by HC.

While it is obvious that flow width and the nature of the endwall boundary layers must be significant parameters, at least when the width is small, the strong

dependence suggested by comparing the results of RF, JF and HM, particularly the non-monotonic behaviour, is not supported by the evidence from HC. Employing end plates to vary the flow width, HC found that the effect on the streamwise Reynolds stress, $\overline{u^2}$, was significant only when the aspect ratio, W/X_A, was less than about unity, implying that $\overline{u^2}$ would not have been much affected in the studies of RF and CH, even though the flow width cannot have been unimportant near the surface (e.g. the surface streamlines of RF). This lack of dependence on flow width casts further doubt on the measurements of JF, which were also questionable on the grounds that the stress levels are unduly large (H. H. Fernholz, private communication) and do not agree well with hot-wire measurements made at the edge of the bubble. Other parameters that are either known to, or are likely to, affect the flow include blockage, Reynolds number, and residual unsteadiness or turbulence in the free stream. The measurements of RF, JF and CH were made at comparable Reynolds numbers, while those of HM and HC were made at a Reynolds number an order of magnitude smaller so as to achieve a high flow width, which necessitated a small fence height. A drawback of pulsed-wire anemometry is that the maximum velocity is limited by probe size, a smaller probe having a smaller maximum roughly in proportion to its size which, with the necessity to keep probe size in relation to the flow as small as possible, limits the maximum velocity. It appeared therefore that, amongst the factors which in principle have influence, the Reynolds stresses must depend significantly on Reynolds number. Indeed, the flow visualization of RF shows a significant change of turbulence structure over the Reynolds number range in question.

The present measurements were made in the rig of JF, using both the original fence and a new, smaller fence, with the purpose of resolving the discrepancies outlined above. The height of the new fence was chosen as a compromise between providing a flow wide enough to be free of end effects, covering the required Reynolds number range, a usable velocity range in the wind tunnel, and available pulsed-wire probes of a size suited to the size of the bubble. The width of the bubble behind the new fence was four bubble lengths, which was just about large enough for end effects to have been negligible. These new measurements show a systematic increase in $\overline{u^2}$ with Reynolds number, concurring with the measurements of RF, CH, HM and HC at the respective Reynolds numbers. Other components of the Reynolds stress tensor were not measured because of the very limited time available for these measurements, but it is argued later that $\overline{u^2}$ is affected more than the other stresses. At low Reynolds numbers in particular there is no reason to suppose that the Reynolds stresses should remain in fixed proportion independent of Reynolds number; indeed the evidence from various flows is to the contrary.

In this type of separated flow the boundary layer upstream of separation is very thin, and far too thin to be measured without special instrumentation. However, as will be seen, its size is not unimportant. An approximate calculation of its overall and momentum thicknesses at separation, δ_o and θ_o, can be made by supposing the external velocity to vary linearly from the stagnation point to a level implied by the pressure just downstream of the fence. Applying the Falkner–Scan analysis leads to $\theta_o/H_f \approx 0.27(U_r H_f/\nu)^{-1/2}$, where H_f is the half-height of the fence front face, and U_r is the free-stream velocity. It follows that the Reynolds number based on the momentum thickness at separation, $U_r\theta_o/\nu$, is given by $U_r\theta_o/\nu \approx 0.27(U_r H_f/\nu)^{1/2}$, implying a range of $U_r\theta_o/\nu$ from $\sim$10 to $\sim$35 for the present measurements. It is appropriate to compare the outer part of the bubble with a mixing layer, as has been done previously, by for example Eaton & Johnston (1981), RF, CH and HM. However, virtually none of the measurements available were made for mixing layers

originating from a boundary layer at such a low Reynolds number. One such set of measurements is that of Lasheras, Cho & Maxworthy (1986), but the data are of limited streamwise extent in a two-stream mixing layer and contain the effects of the near wake. Therefore, a few measurements were also made in a mixing layer of Reynolds number comparable to the above range.

2. Experimental apparatus and measuring techniques

The separation-bubble measurements were made in the low-speed wind tunnel of the Hermann–Föttinger Institut, which has a working section width and height of 2.0 m × 1.4 m, respectively. The splitter plate, which was 10 mm thick and 2 m long, was mounted vertically in the centre of the working section with its upstream edge about 5 m from the contraction exit, as employed by JF. The original fence had a height, h_f of 22.0 mm above the splitter plate surface, making an overall fence height, $2H_f$, of 54 mm. The new fence, employed for the bulk of the measurements, had a height (h_f) of 11.0 mm above the splitter plate surface and therefore an overall height of 32 mm. For probe calibration purposes the fence was removed and replaced with a profiled leading edge. A reference Pitot static probe was placed well above the separation bubble, and second reference Pitot static probe was placed near the contraction exit as in JF. A reference static pressure on the splitter plate surface was also taken at 510 mm from the fence. The free-stream velocity (at the reference point above the bubble) was varied between 1.6 m s^{-1} and 16.4 m s^{-1}.

The pulsed-wire probe was supported from the 'underside' of the plate, and passed through one of the instrumentation ports placed at intervals along the centreline. The first port on the centreline was 44 mm from the fence front face, and the remainder were at intervals of 50 mm. Further details are given by JF. Profiles were measured at the stations nearest to $x/X_A = 0.25$, 0.5, 0.75, 1.0 and 1.25, with most nearest to 0.5 and 1.0 behind the smaller fence.

Standard pulsed-wire velocity probes of the type described by RF, CH and JF were used for some of the measurements behind the larger fence, the remainder being made with 'miniature' pulsed-wire probes identical to those used by HC and HM. For the smaller fence only the miniature probes were employed. These had pulsed- and sensor-wire lengths of about 6 mm, and a distance between pulsed- and sensor-wire of about 0.7 mm, that is, about half the dimensions of the standard probe. The pitch and yaw responses were in excess of $\pm 80°$, and $\pm 70°$, respectively. For some of the probes the sensor wires were offset as described by CH, although there were no significant differences in the measurements from these and the other probes. There was no significant difference between the measurements behind the larger fence from the standard and miniature probes, their relative sizes implying the miniature probes were also adequately small for the flow behind the smaller fence. The errors arising from incomplete cosinal response are discussed by Castro & Cheun (1982), where they indicate that the error in $\overline{u^2}$ should be better than $\pm 10\%$ for the present measurements.

One of the problems with pulsed-wire velocity measurements is that tight wires usually lead to high levels of 'strain-gauge' noise generated by mechanical vibration from the turbulence itself, or from the wind tunnel. The best remedy, as established by Bradbury & Castro (1971), is to make a small kink at one end of each sensor wire and preferably the pulsed wire also, because this transmits vibration as it is pulsed. Alternatively, and more easily, slightly loose wires can be used (Jaroch 1985), but these leave some uncertainty in the reliability of the calibration, though in none of

the measurements made in the present work did wire looseness account for anything like the high level of $\overline{u^2}$ measured by JF. All the measurements presented here were made with kinked wires held in slight tension.

Two wall shear-stress probes were employed, each having sensor-wire lengths, l, of about 0.5 mm, giving lu_τ/v not exceeding about 15, where u_τ is the friction velocity. The probe with the larger wire height of 90 μm was used at the lower Reynolds numbers because a greater height is then permissible, and because the signal strength from the 50 μm height probe was too small. In the region of overlap the two probes gave equal measurements. The yaw response of this type of probe is very closely cosinal, to an angle better than $\pm 85°$. One of the difficulties encountered in spanning the present Reynolds number range is that a change of one order of magnitude in free-stream velocity implies, all else constant, a change of two orders of magnitude in mean wall shear stress. Such a range, together with the high intensity of the fluctuations, is demanding of pulsed-wire anemometry, although some alleviation of the required calibration range is given by the decrease in wall shear stress with increase in Reynolds number. The probes were calibrated against Preston tubes in a zero-pressure-gradient turbulent boundary layer using the calibration of Patel (1965). Pressures were measured using a Baratron temperature-compensated pressure transducer, having a resolution of 0.01 Pa.

Nearly all the pulsed-wire measurements were made using a PELA-Flow Instruments anemometer unit and LabView-based software written at Surrey and run on a Macintosh computer interfaced via a National Instruments LabNB board. The calibrations for velocity and shear stress were mostly fitted to third-order polynomials, namely

$$U, \tau_w = A + B\frac{1}{T} + C\frac{1}{T^2} + D\frac{1}{T^3}, \tag{1}$$

where T is the instantaneous time of flight; it was generally found better not to require A to be zero. Some measurements were also made using the HFI version of the anemometer unit and associated software run on an Atari-type computer; the two systems gave identical results. In order to ensure satisfactory accuracy two sets of calibrations were made, one for the full velocity or shear stress range and the other for a lower range, the latter giving a better fit at lower velocities or wall shear stress. One or other calibration for each sensor was selected (prior to measurement, not dynamically) according to the range of the positive and negative fluctuations. Departures between the 'true' velocity or wall shear stress and the calibration curves were negligible.

There is a level of velocity and shear stress below which pulsed-wire anemometry cannot measure because even in the absence of a timer limitation (which in practice may or may not occur first) thermal diffusion reduces discrimination of the heat trace. However, it is possible to make a correction for this 'blind zone' by interpolation across the 'hole' on the probability density function (p.d.f.). The p.d.f. was recorded for each measurement and a two-piece linear interpolation was made so as to preserve the area under the p.d.f. The resulting adjustments were in fact negligible, except for the reverse-flow fraction, where the error arises largely because of the ambiguity in sign of undetected traces. Typically 80 bins were used for the p.d.f., though some given here have been smoothed to 20 bins.

As shown by Castro, Dianat & Bradbury (1987) and Dengel, Fernholz & Hess (1986) the effect of the finite length of the shear stress probe wires (as opposed to zero length) is to reduce the probe's sensitivity to shear stress fluctuations as a

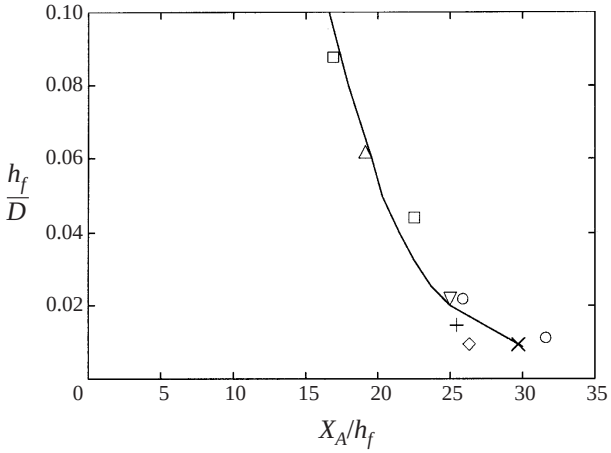

FIGURE 1. Variation of attachment length with blockage. □, RF; ◇, HM; △, CH; ▽, JF; +, HC; ×, Hancock (1999); ○, present, small and large fences. Line from Smits (1982).

consequence of spatial averaging, the net effect on the mean level being negligible. Castro *et al.* advise that lu_τ/ν should be less than 30, based on measurements in a zero-pressure-gradient turbulent boundary layer. Pessimistically, their measurements imply that the error for the present probe will not have exceeded 8%. However, Hancock (1999) concluded that the error beneath a separated flow must be significantly less because the fluctuations are predominantly large-scale fluctuations arising from the 'inactive' motion (Townsend 1976) imposed by the intense outer-layer structures (see also Fernholz 1994). The present errors will have been considerably less than the above estimate, therefore.

The mixing layer measurements were made in a 0.6 m × 0.3 m blower wind tunnel at the University of Surrey. The mixing layer was formed on a 20 mm or 40 mm long plate held just above the contraction-exit boundary layer which was bled off beneath the plate. Measurements were made using a digitally linearized, single-wire, hot-wire anemometer, driven by a Dantec DO1 anemometer unit. The free-stream speed was varied between 2.5 m s^{-1} and 5 m s^{-1}, and the velocity profiles at the separation point showed very good agreement with the Blasius profile, to a deviation better than 1% of the free-stream velocity. Data acquisition was achieved using a similar system to that used for the pulsed-wire anemometry.

3. Results and discussion

3.1. *Preliminary matters*

Unless otherwise stated, the reference velocity for previous measurements has been redefined to that used here, namely the free-stream velocity above the position of attachment. In some instances a large adjustment has been made, but no sensible comparison would be possible without such a redefinition; no information is lost by it, of course.

Figure 1 shows the effect of blockage on attachment length, X_A, for the present and previous measurements, together with the variation from Smits (1982; see also CH). X_A is the distance to attachment on the flow centreline, and the term 'attachment' is used in this paper in preference to the term 'reattachment' because although the

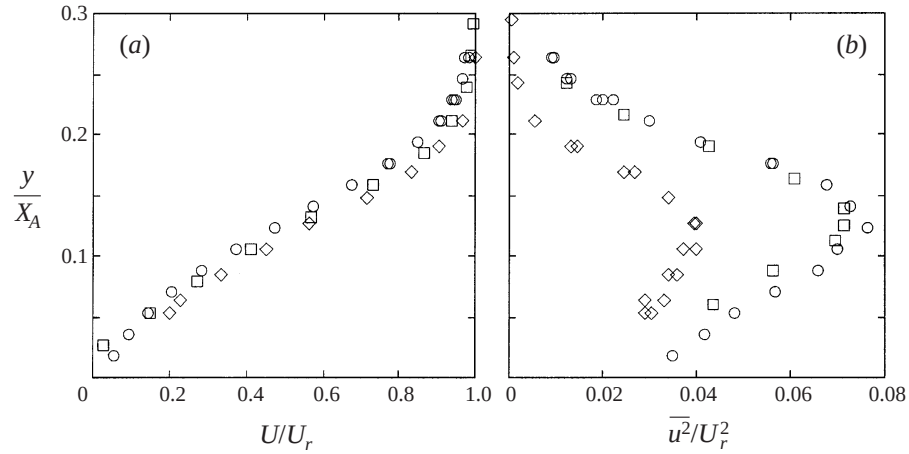

FIGURE 2. Profiles of (*a*) U and (*b*) $\overline{u^2}$ at $x = X_A$. □, RF; ◇, HM; ○, present, large fence.

flow reattaches the separating streamline is only a reattaching streamline if the flow is genuinely invariant with lateral position, z. As noted in the Introduction the widths of most of the sets of measurements discussed here were too small for the bubbles to have met this condition. The attachment lengths given in table 1 were not in all cases confirmed by an equal length on the 'underside', and although the models were all nominally parallel with the upstream flow, some caution should be attached to X_A when comparing it with h_f. In the present case symmetry could not be employed as a test because the instrumentation plugs protruded on the underside of the splitter plate. The flaps at the rear of the splitter plate were left in one position, though ideally they would have been set each time the fence was changed so as to give a preferred attachment length. For the smaller fence X_A is 20% larger than it was for HM, and 10% larger than that from Smits (1982) and from Hancock (1999), but, as will be seen from the consistency of the measurements presented later, there is no reason to believe that this difference is of any material significance.

The first of the present measurements were made downstream of the original fence with conditions as identical as possible to those of JF. The wall shear stress measurements agreed very well with their results, which gave an X_A of 570 mm as opposed to 549 mm here, i.e. within 4%. Figure 2 shows U and $\overline{u^2}$ near attachment, where U is the mean velocity in the free-stream direction. U is quite comparable with that measured by JF (not shown); $\overline{u^2}$ by contrast is very close to that measured by RF and therefore very much less than measured by JF. Measurements were made with several probes with various degrees of wire tightness and condition and a number of threshold settings and sensor-wire currents, using both the PELA-Flow and HFI instruments, but it was not possible to obtain the levels of $\overline{u^2}$ measured by JF. In fact the largest departure at attachment was no more than about 10% higher than given in figure 2(*b*), and no explanation for the much higher levels reported by JF could be found.

The bubble behind the larger fence was slightly thicker than that behind the smaller fence, after scaling on bubble length or fence height. HC found that if the aspect ratio is less than about 2 the bubble height in the centre is larger than in a wider flow, the main effect being an outward displacement of the free shear layer as inferred from the displacement of the profile of the streamwise velocity, U. The profile of $\overline{u^2}$ is displaced by a similar amount, but with little change in shape and negligible

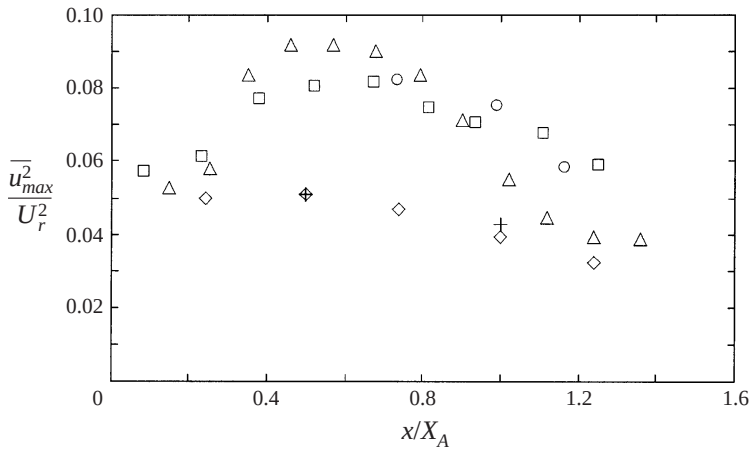

FIGURE 3. Variation of $\overline{u^2_{max}}$ with x/X_A. □, RF; ◇, HM; △, CH; +, HC; ○, present, large fence.

change in magnitude. This displacement effect is less marked in RF (e.g. figure 2*a*) even though the aspect ratio is less than half that of the present large-fence flow. It is supposed that these differences are a consequence of the relatively thick boundary layers on the working section walls owing to the distance of the flow rig from the contraction exit, and the relatively thin boundary layers in the case of RF, their fence having been close to the contraction exit. The measurements behind the smaller fence are consistent with the flow having been wide enough for end effects to have been negligible.

Figure 3 shows the streamwise development of the maximum in $\overline{u^2}$, $\overline{u^2_{max}}$, according to the measurements of RF, CH, HM and HC, the present measurements concurring with those of RF. Two noteworthy points come from this figure and figure 2. First, although the blockage in the experiment of RF was much larger than here, and the bubble height and length markedly less (by about 35%), the shapes of the profiles of U and $\overline{u^2}$ are very similar when normalized by the bubble length, with very close maxima in $\overline{u^2}$. This concurrence underlines the established view that it is the attachment length rather than the fence height that provides the primary scale of the bubble, if the fence height is relatively small. The second point, the issue of primary concern here, is that the difference between the measurements of HM and HC and the remainder of the measurements in these two figures is seen over two-thirds of the bubble, the marked departure taking place between roughly $0.2X_A$ and $0.4X_A$. The measurements of CH differ significantly near and after attachment, though there is no clear reason why there should be such a difference. A possible explanation is offered shortly.

The outer free shear layer part of a separation bubble is at least in simple terms a mixing layer subjected to an extra rate of mean strain arising from curvature of the mean streamlines, and to fluctuating rates of strain imposed on the 'low-speed' side by the fluid entrained from near attachment. (HM argue that curvature effects should be small in the outer part.) This connection leads to a velocity scale for the shear layer as being the maximum velocity difference, ΔU, across the bubble, where $\Delta U = U_{max} - U_{min}$, disregarding the near-wall layer where the viscous constraint dominates. Inconsistently, in previous work, the near-wall layer has not been ignored in forming the velocity difference *downstream* of attachment, where the minimum in $U(y)$ is zero, of course. A consistent and more sensible velocity difference, $\Delta U'$, is given

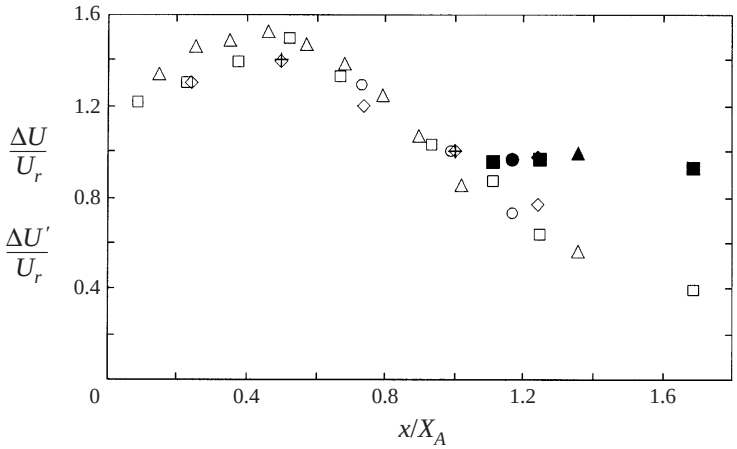

FIGURE 4. Variation of $\Delta U/U_r$ (closed symbols) and $\Delta U'/U_r$ (open symbols) with x/X_A. Symbols as in figure 3.

by $\Delta U' = U_{max} - U_i$, where U_i is the velocity just outside the near-wall layer. Upstream of attachment U_i is taken as U_{min} (so that $\Delta U = \Delta U'$) while downstream U_i is judged as the velocity where the gradient is negligible in terms of the velocity variation in the near-wall layer. Such a definition of an 'edge velocity' is of course approximate, as is the definition upstream of attachment (where there is also an external velocity gradient), but a more exacting definition would not differ significantly in consequence in the present context. Figure 4 shows $\Delta U/U_r$ and $\Delta U'/U_r$, where it is interesting to note that $\Delta U'/U_r$ continues to decrease at the same rate after attachment as before, in contrast to $\Delta U/U_r$, which shows an abrupt change. It should perhaps be mentioned that U_i was not selected so as to give the linear variation seen in this figure, or to force any of the other inferences drawn later. The maxima in $\overline{u^2}$ normalized by ΔU and by $\Delta U'$ are shown in figure 5, where a very different behaviour is portrayed beyond attachment, $\overline{u^2}$ continuing to rise when normalized by $\Delta U'$. Interestingly, the measurements of CH as given in figure 5(*b*) are much closer to those of RF† and the present measurements. In that $\overline{u^2}/\Delta U'^2$ is formed entirely from one measurement source, namely the pulsed-wire probe, this closeness does suggest some sort of error in the measurements of CH that is not apparent when $\overline{u^2}$ is normalized by $\Delta U'^2$. (This figure lacks the two points between $x/X_A = 1.1$ and 1.3, because U_i is not available for these stations.) $\overline{u^2_{max}}/\Delta U^2$ in a developed plane mixing layer is about 0.029.

3.2. *Wall pressure and shear stress*

The distance to attachment, X_A, varied only a small amount with free-stream velocity, as shown in figure 6, though for reasons given earlier this should not be taken as an indication of how attachment length varies with Reynolds number. Indeed, none of the available data suggest a significant variation over the present range. Here, X_A was within $\pm 4\%$ of 349 mm. Figure 7 shows the variation of the surface pressure distribution, C_p, with x/X_A. C_p is defined as $C_p = 2(p - p_o)/\rho U_o^2$, where p_o is the surface pressure downstream of attachment (at about $1.5X_A$), and U_o is a notional free-stream velocity based on p_o and the free-stream total pressure. U_r/U_o is 1.06. The variation of C_p with Reynolds number is at most slight and confined to the

† Data in figures 18 and 20 of RF are inconsistent for $x/X_A > 1.2$. Present data from H. H. Fernholz, private communication, are consistent with figure 18.

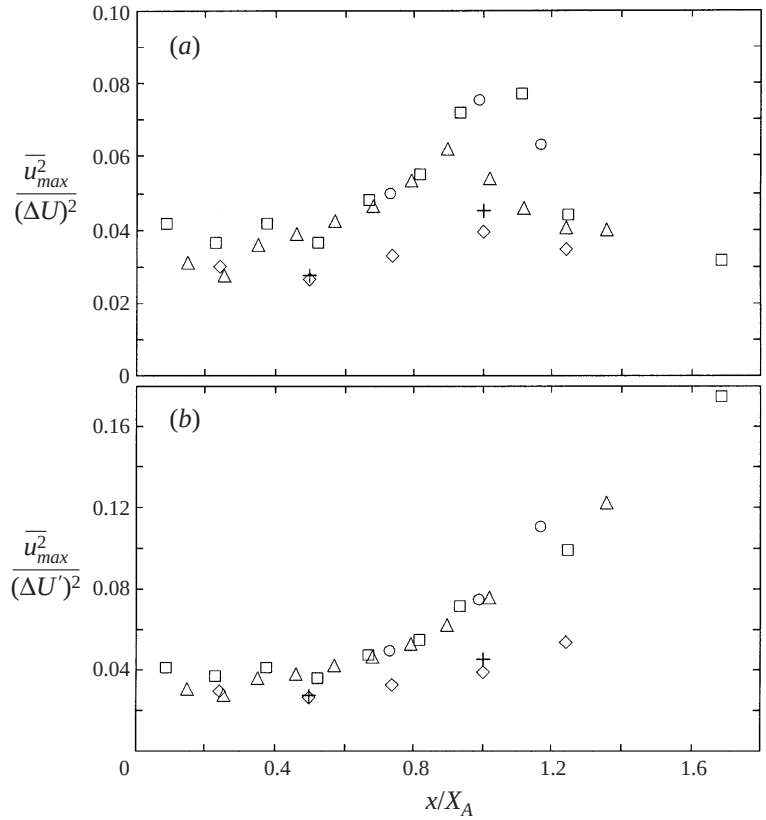

FIGURE 5. Maximum in $\overline{u^2}$ normalized by (*a*) ΔU and (*b*) $\Delta U'$. Symbols as in figure 3.

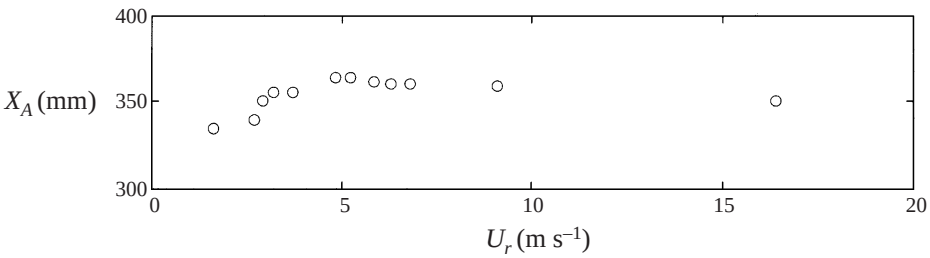

FIGURE 6. Variation of attachment length with reference velocity, downstream of the small fence.

lowest Reynolds number, and is consistent with the mean flow features remaining very nearly constant.

Figure 8 shows the mean wall shear stress coefficient, C_f, and the coefficient of the r.m.s. of the shear stress fluctuations, C'_f, defined as $2\overline{\tau_w}/\rho U_r^2$ and $2\tau'_w/\rho U_r^2$, where $\overline{\tau_w}$ and τ'_w are the mean shear stress and r.m.s. of the fluctuation, respectively. Clearly, the magnitude of the wall stress decreases markedly as the Reynolds number increases, and this is shown again in figure 9 in terms of the peak negative mean wall stress. CH observed a similar trend with a very similar form of distribution, though their corresponding levels are considerably higher than here (where their data have been adjusted to the same reference velocity as that used here). The measurements of RF

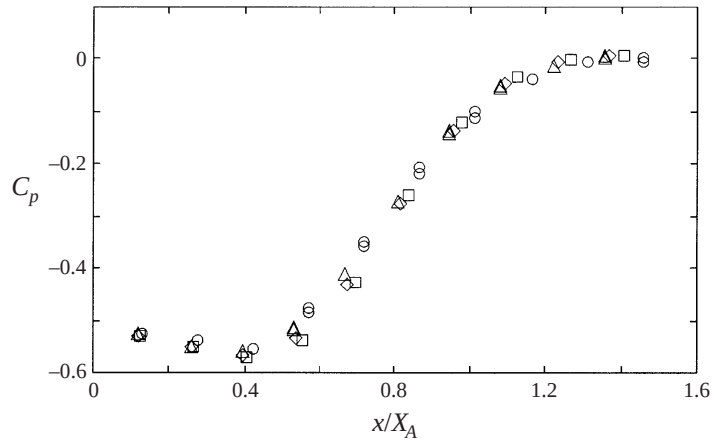

FIGURE 7. Variation of surface pressure, C_p, with Reynolds number. ○, $U_r h_f/\nu \times 10^{-3} = 2$; △, 3.5; ◇, 6.7; □, 12. Small fence.

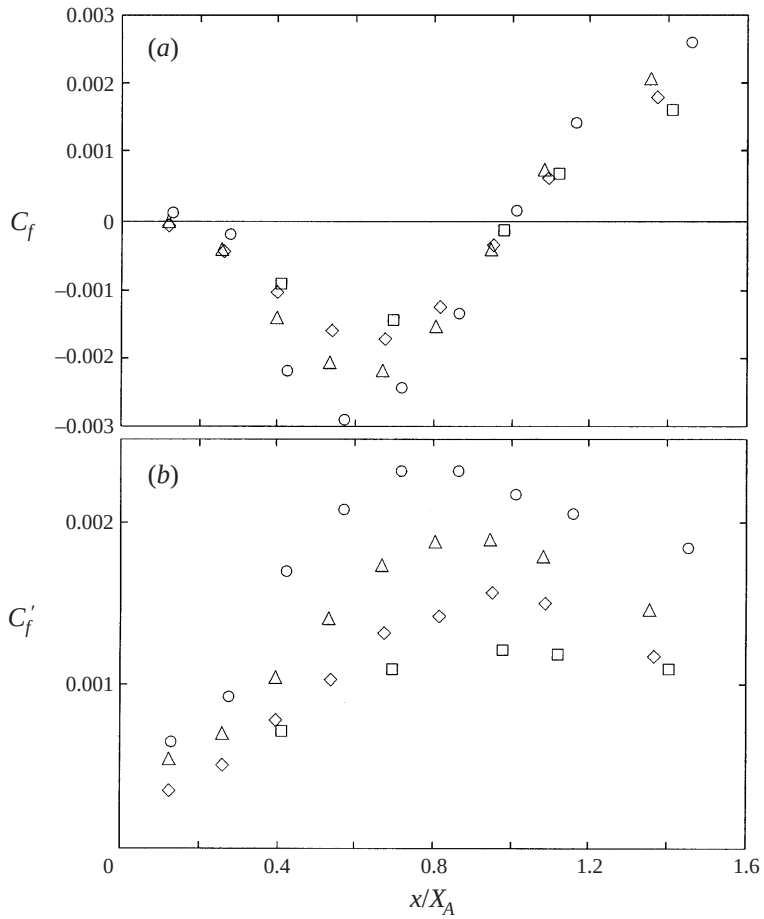

FIGURE 8. Variation with Reynolds number of (*a*) mean surface shear stress coefficient, C_f and (*b*) r.m.s. of surface shear stress fluctuation, C_f'. Symbols as in figure 7.

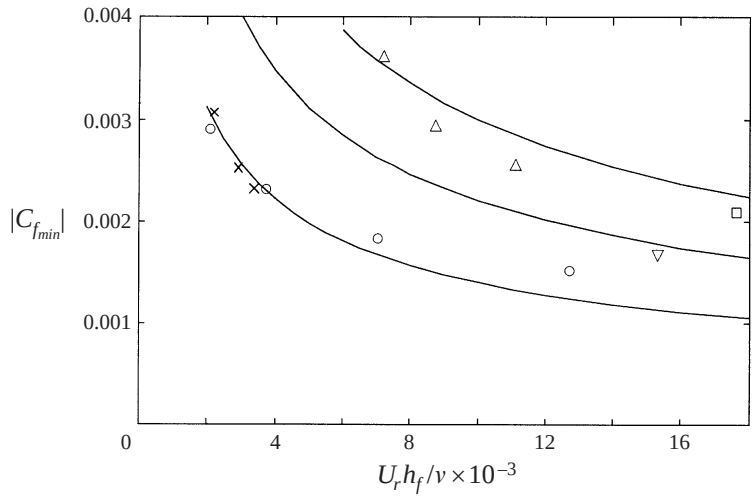

FIGURE 9. Variation of peak negative mean surface shear stress with Reynolds number. □, RF; △, CH; ▽, JF; ×, Hancock (1999); ○, present, small fence. Lines correspond to $|C_{f_{min}}|$ varying as $(U_r h_f/\nu)^{-1/2}$.

are also larger by about the same factor while the measurement of JF (as confirmed here) is much closer to the trend with the small fence. As discussed further later, the substantial discrepancy in figure 9 is an effect of flow width, where the higher wall shear stress at low aspect ratio is a consequence of differences in the near-wall flow, rather than errors in measurement. The present C_f are very close to the measurements of Hancock (1999) in a wider flow of $W/X_A = 5.7$ (very nearly identical to that of HM), as shown in figure 9, consistent with the view that the present flow was about wide enough for end effects to have been negligible. (In Hancock's flow a width in excess of $1.4X_A$ was free of significant end effects, as inferred from measurements of wall shear stress.)

The variation of C_f with Reynolds number seen here is comparable with that of Jovic & Driver (1995, see also Le, Moin & Kim 1997) in a separation bubble behind a rearward-facing step. Moreover, the dependence here explains the large C_f seen in the direct numerical simulations of Le *et al.* (1997) – namely that C_f increases with decreasing Reynolds number. A further point about figure 8 is the longer secondary separation bubble and the slightly earlier occurrence of the peaks in C_f and C_f' at the lowest Reynolds number. The latter is presumably connected with the slightly earlier rise in C_p.

The fluctuating shear stress normalized by the (negative) peak level of the mean shear stress, $|C_{f_{min}}|$, is shown in figure 10. As can be seen, these collapse closely to a single curve apart from a slight departure at the lowest Reynolds number. The lack of any departure in the vicinity of the secondary separation is perhaps surprising because presumedly in this region the distance to secondary separation is also a relevant length scale. However, the conclusion of Hancock (1999) that the surface fluctuations are predominantly a result of large-scale motion in the outer flow explains the lack of dependence on the length of the secondary separation bubble. In addition, Hancock showed that the mean and fluctuating shear stresses are not directly linked, so the constancy in figure 10 is therefore notable. $C_f'/|C_{f_{min}}|$ as measured by RF is comparable with that here, while JF obtained levels that were roughly 25% larger.

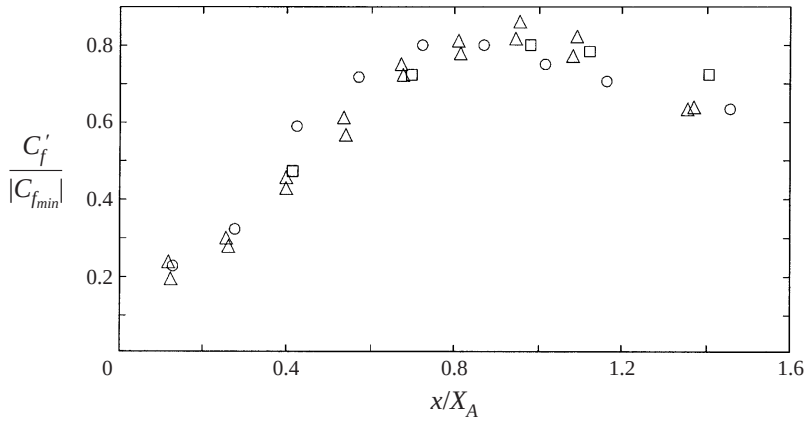

FIGURE 10. C_f' normalized by the peak negative mean shear stress. Symbols as in figure 7.

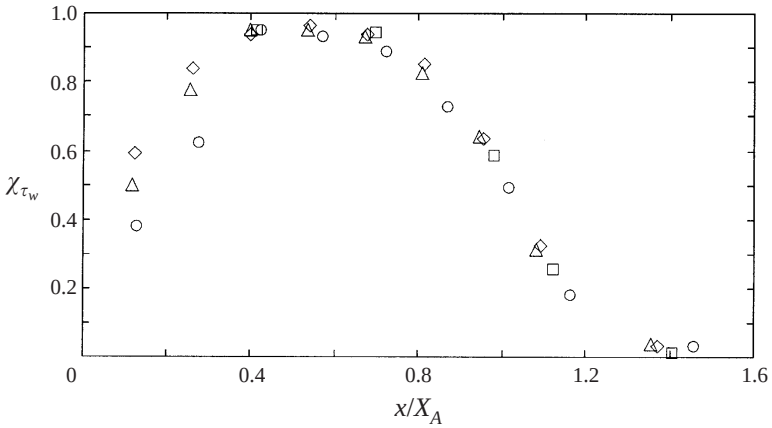

FIGURE 11. Reverse-flow factor, χ_{τ_w}. Symbols as in figure 7.

The reverse-flow fraction for the wall shear stress, χ_{τ_w}, defined as

$$\chi_{\tau_w} = \int_{-\infty}^{0} p(\tau_w)\,\mathrm{d}\tau_w, \tag{2}$$

where $p(\tau_w)$ is the probability density function of the (x-direction) wall shear stress, and where the integral over all τ_w is unity, is shown in figure 11. In this definition, τ_w is the instantaneous total wall shear stress in the x-direction, as measured directly by the pulsed-wire probe. Two immediate observations are that downstream of about $x/X_A = 0.4$, there is no significant change with Reynolds number, and that χ is very close to 0.5 at attachment. There is no obvious reason why the reverse-flow fraction should be equal to one-half at the point where the mean wall shear stress is zero, though very nearly all measurements show it to be so. Upstream of $x/X_A = 0.4$ there is a clear variation with Reynolds number, where the position of secondary separation in figure 8(*a*) again compares closely with $\chi = 0.5$. The shape of $p(\tau_w)$, scaled on τ_w', also does not change with Reynolds number, as shown for example in figure 12, for $x/X_A \approx 0.55$, where in this figure τ_w is taken with respect to the mean level. The case at the lowest Reynolds number differs from the others near where the total wall stress is zero (i.e. near where $\tau_w/\tau_w' = +1.03$) but this difference is consistent with the

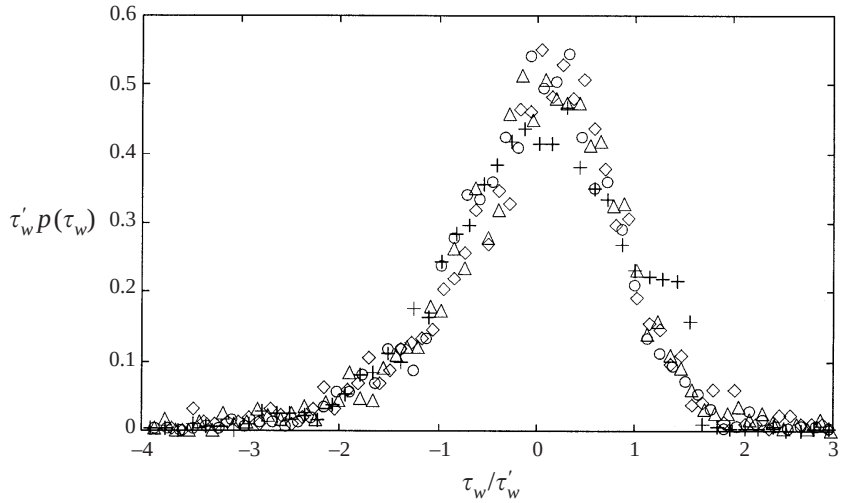

FIGURE 12. $p(\tau_w)$ at $x/X_A \approx 0.5$. +, $U_r h_f/\nu \times 10^{-3} = 1.2$; ○, 2; △, 3.5; ◇, 6.7. Small fence.

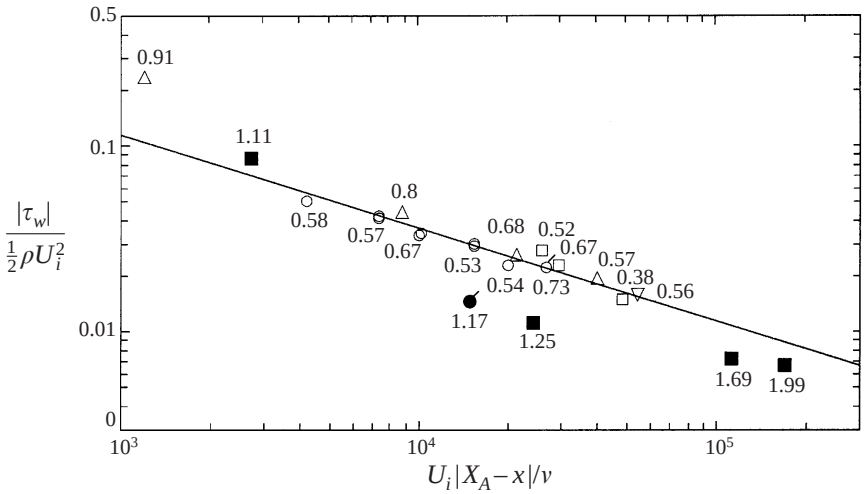

FIGURE 13. C_{f_i} as a function of $U_i|X_A - x|/\nu$. Numbers denote x/X_A. □, RF; △, CH; ▽, JF; Present: ○, small fence; ◌́, large fence. Closed symbols are for $x/X_A > 1$. Line is $C_{f_i} = 3.6(U_i|X_A - x|/\nu)^{-1/2}$.

inaccuracy in the probe calibration at the lowest levels; at higher levels the differences are negligible, suggesting the p.d.f. as a whole is unchanged at the lowest Reynolds number in this figure.

The behaviour of the near-wall layer is more appropriately described in terms of the 'free-stream' velocity, U_i, near its edge and its development length from the attachment position. Several workers have demonstrated that for the reverse flow this comparatively thin layer behaves in a viscous-dominated manner (e.g. Adams & Johnston 1988; Devenport & Sutton 1991; Dianat & Castro 1989). Figure 13 shows the present measurements and those of RF, JF and CH, where C_f is now defined as $2|\overline{\tau_w}|/\rho U_i^2$ and the Reynolds number as $U_i|X_A - x|/\nu$. This figure also includes some measurements downstream of attachment where, at least not too far from attachment, the near-wall layer must have some similarities with that beneath the recirculating

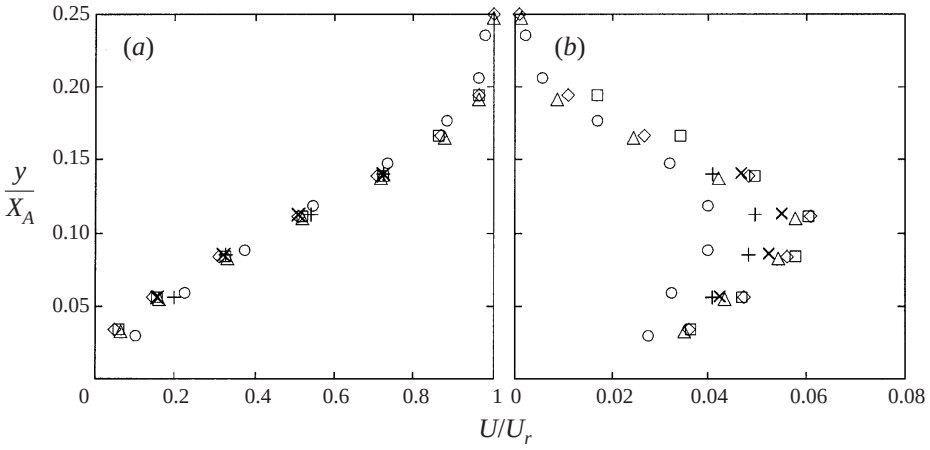

FIGURE 14. Profiles of (*a*) U and (*b*) $\overline{u^2}$ at $x = X_A$. ○, $U_r h_f/\nu \times 10^{-3} = 2.0$; +, 2.3; ×, 2.7; △, 3.5; ◇, 4.6; □, 6.7. Small fence.

flow. Upstream of attachment, the measurements exhibit a slope closely equal to $-1/2$, except near the attachment position itself, where the gradient is steeper. If U_i and X_A were both precisely independent of Reynolds number then a variation of C_f as $(U_i(X_A - x)/\nu)^{-1/2}$ would imply a variation of $C_f = 2|\overline{\tau_w}|/\rho U_r^2$ according to $(U_r h_f/\nu)^{-1/2}$. However, as can be seen from figure 9, the present measurements do not follow this form of variation. The mean flow cannot therefore be entirely independent of Reynolds number, and indeed it is to be expected that U_i would depend upon how far the near-wall layer grows into the flow above. (The layer is too thin for its thickness to be determined accurately from the data being considered here.) Downstream of attachment C_f varies in a different manner presumably reflecting the different pressure gradient.

A further point from figure 13 is that the various measurements either side of attachment are very much closer together than are the measurements in figure 9, independent of aspect ratio. In that the quantities employed in figure 13 are appropriate to the near-wall layer the agreement between the various sets gives confidence in the accuracy of the measurements in each case, implying that the differences seen in figure 9 are indeed a genuine effect of aspect ratio. The effects of low aspect ratio are therefore substantially larger on the wall shear stress and the near-wall flow than they are on the outer flow, as inferred from HC, the present results implying that W/X_A should be about 4 for end effects to be negligible (figure 9). The sensitivity of the near-wall flow arises, at least in part, because its low momentum means it is relatively easily influenced by the residual lateral pressure gradient (see JF) imposed by the outer flow.

3.3. *Mean velocity and Reynolds stress*

Figure 14 shows U and $\overline{u^2}$ at $x/X_A = 1$, where the variation of $\overline{u^2}$ with Reynolds number is about its largest. The small but noticeable variation in U in this figure arises because of the slight variation in X_A in relation to the fixed instrumentation positions. By contrast, $\overline{u^2}$ changes significantly over the relatively small change in Reynolds number in this figure, the change being predominantly one of change of magnitude, the shape remaining about constant.

The variation in $\overline{u^2}$ can be summarized conveniently in terms of its maximum, as

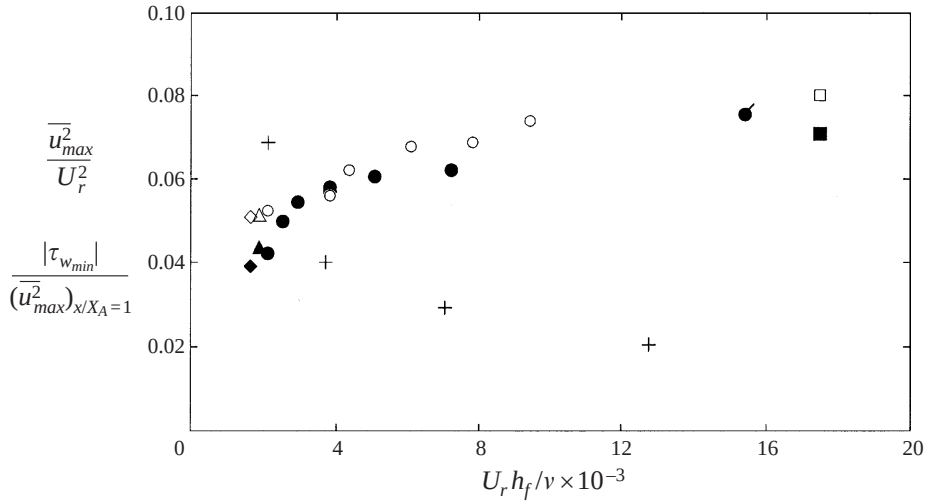

FIGURE 15. Variation of $\overline{u^2_{max}}/U_r^2$ with $U_r h_f/\nu$. □, RF; ◇, HM; △, HC; Present: ○, small fence, ●, large fence. Open symbols, $x/X_A = 0.5$. Closed symbols, $x/X_A = 1$. The figure also shows +, $|C_{f_{min}}|/(\overline{u^2_{max}}/U_r^2)_{x/X_A=1}$.

shown in figure 15, for $x/X_A = 0.5$ and 1, where it can be seen that the present variation agrees very well with the measurements of HM, HC and RF. This variation is strongest at the lowest Reynolds number and suggests, as would be expected, that $\overline{u^2_{max}}$ remains constant at high Reynolds number. The agreement with previous measurements is important in a number of respects. The agreement with HM and HC confirms that the flow was wide enough for end effects not to have affected U or $\overline{u^2}$ in the bulk of the bubble. The agreement is an example of how the dependence of the flow on blockage and other parameters (e.g. a small, non-zero circulation around the plate) is of no consequence in the immediate context of the Reynolds-number dependence of $\overline{u^2}$. The agreement with RF gives confidence in at least some features of their measurements as representative of a two-dimensional flow. Therefore, it is clear from this figure that the variations seen in the earlier measurements, as shown in figures 1, 3 and 5, are primarily a dependence on Reynolds number. Figure 15 also shows $|C_{f_{min}}|$ normalized by $\overline{u^2_{max}}$ at attachment, which is seen to decrease with increasing Reynolds number. Given the near constancy in figure 10 it follows that C_f' normalized by $\overline{u^2_{max}}$ at attachment decreases in a similar manner; $\overline{u^2_{max}}$ is not a scale for C_f', therefore (though Hancock 1999 shows C_f' to be determined largely by outer-flow structures, uncoupled from the mean wall stress, C_f).

The growth of a mixing layer can be defined in terms of the maximum velocity gradient, $(\partial U/\partial y)_{max}$, normalized by a characteristic velocity difference. Previous workers have used a gradient (or 'vorticity') thickness, L, defined by $L = \Delta U/(\partial U/\partial y)_{max}$, whereas, for the reasons cited earlier, the definition preferred here is the thickness, L', defined by $L' = \Delta U'/(\partial U/\partial y)_{max}$, where upstream of attachment L and L' are equal, of course. Figure 16 shows both L and L' for the present and previous measurements. Until about $x/X_A = 0.7$ the thickness grows linearly at a rate comparable with that of a plane mixing layer (e.g. Johnson & Hancock 1991). The reduction in growth rate of L' near and after attachment as opposed to the decrease and subsequent increase of L over and above that in the earlier part of the bubble adds to the appropriateness of using L' in preference to L because a lower growth rate downstream of attachment

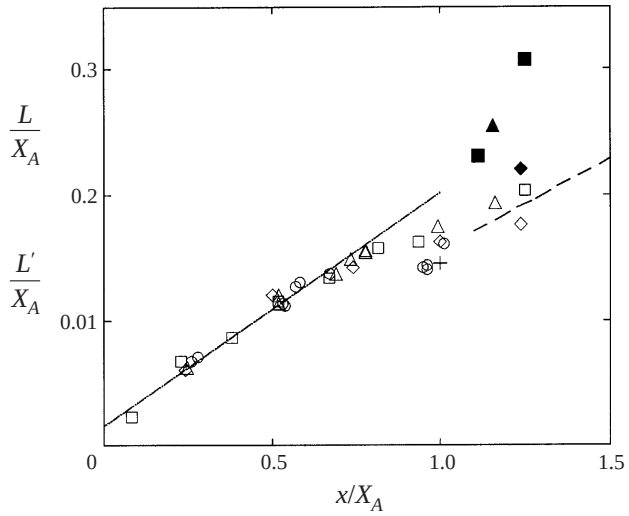

FIGURE 16. Gradient thicknesses, L (closed symbols) and L'. □, RF; ◇, HM; +, HC; Present: ○, small fence, △, large fence, all Reynolds numbers. Full line is growth rate of plane mixing layer, 0.186. Broken line is growth rate of 0.145.

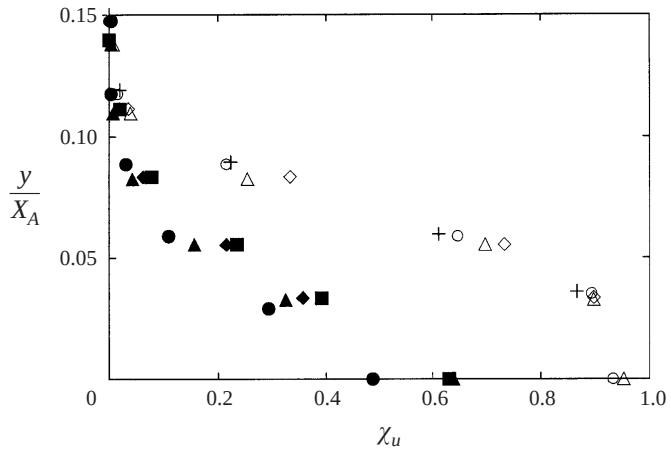

FIGURE 17. Reverse-flow factor, $\chi_u(y)$. +, $U_r h_f/\nu \times 10^{-3} = 1.2$; ○, 2.0; △, 3.5; ◇, 4.7; □, 6.7. Small fence. Open symbols, $x/X_A \approx 0.55$. Closed symbols, $x/X_A \approx 1$. Wall values taken from figure 11.

is *prima facie* more plausible. A reduction of length scale as seen in the behaviour of L' is consistent with the cessation of pairing observed by Cherry, Hillier & Latour (1984), whereas the behaviour of L is not. Also, the fluid that becomes part of the reverse flow in order to supply the entrainment requirement leads to a decrease in the size of the shear layer structures that are carried downstream of attachment. The interpretation here is that the 'torn-off' fluid that is carried upstream is low-momentum fluid of a scale rather less than that of the structures near attachment. For although the growth rate of L' decreases rapidly between x/X_A of ~0.8 and ~1, to roughly one-half that further upstream, the surviving outer-flow structures downstream of attachment as inferred from the overall decrease in L' are reduced in size by only about 20%. Consistent with the near constancy of the mean flow neither L' nor L change noticeably with Reynolds number.

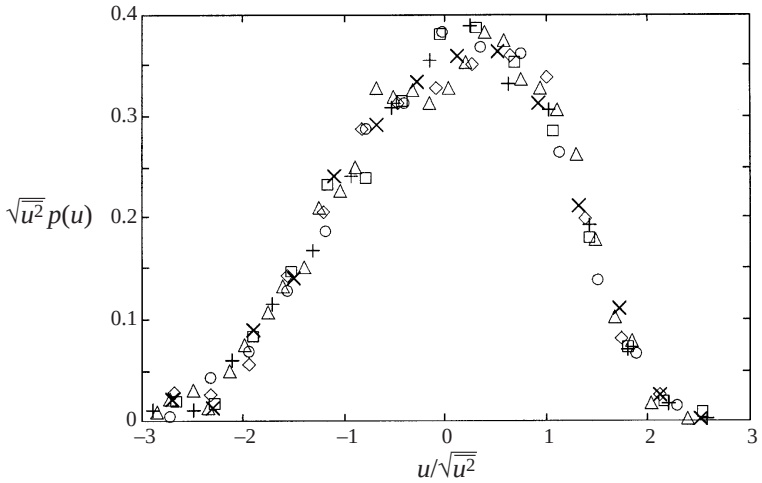

FIGURE 18. $p(u)$ at $x/X_A = 1$ and $y/X_A = 0.11$. ○, $U_r h_f/\nu \times 10^{-3} = 2.0$; +, 2.4; ×, 2.8; △, 3.6; ◇, 4.8; □, 6.7. Small fence.

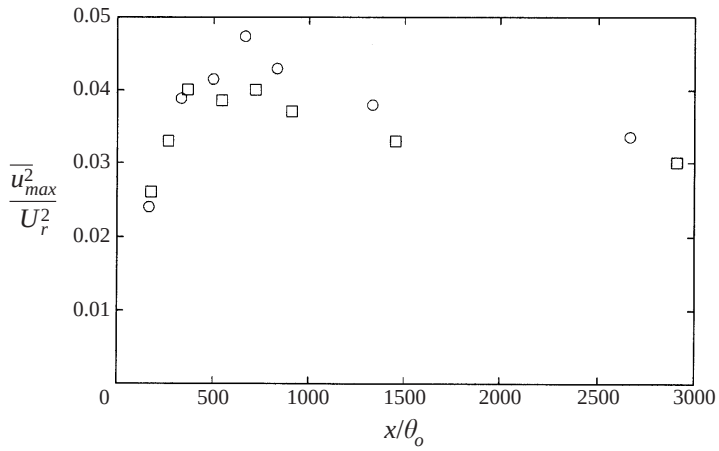

FIGURE 19. $\overline{u^2_{max}}/U_r^2$ in a plane mixing layer. ○, $U_r\theta_o/\nu = 40$; □, 74.

The reverse flow fraction, χ_u, defined for velocity in a similar manner to that for shear stress described by equation (2), is shown in figure 17 for two positions along the bubble, one at about $x/X_A = 0.5$ and the other near attachment; χ_u must of course tend to the wall value as given by the shear stress measurement, χ_{τ_w}, which is included in the figure. The apparent variation with Reynolds number in the measurements near attachment can be entirely attributed to the small variation in the attachment position and the rapid change in χ_u with x at this position, as can be seen from the variation at the wall in figure 11. At the mid position, where a greater dependence might be expected, the variation in χ_u is negligible. Figure 18 shows the p.d.f. at the height near attachment where $\overline{u^2}$ is a maximum. Structural changes with Reynolds number might be expected to lead to changes in the p.d.f., but here the summary measure of the reverse-flow fraction and the p.d.f. itself show no more than a very slight change.

As is of course well known, the initial part of a mixing layer must scale upon a

length scale such as the momentum thickness, θ_o, at separation, and the distance, x, from separation. (Further downstream, after the initial history is lost, the boundary-layer scale can be replaced in terms of dimensional dependence by a virtual origin.) Figure 19 shows the development of the maximum in $\overline{u^2}$ with x for $U_r\theta_o/\nu = 40$ and 74, the first corresponding to $U_r h_f/\nu$ of approximately 26×10^3 and only slightly beyond the upper limit of the other measurements presented here. While there is some dependence on Reynolds number in figure 19 the variation is fairly small. At $U_r\theta_o/\nu = 74$ the asymptotic level is achieved after about $x = 2000\theta_o$, a distance comparable to that at high Reynolds number (Johnson & Hancock 1991). The peak levels, occurring between x/θ_o of about 350 and 700, are also much as at high Reynolds numbers. At $U_r\theta_o/\nu = 40$ a longer distance is required to reach the same asymptotic level. Comparing the level of $\overline{u^2}$ seen in this figure with that seen in figure 15 shows that the high level of $\overline{u^2}$ in the separation bubble arises because of a fundamental difference between the mixing layer lying above a separation bubble and an isolated plane mixing layer, one that is dependent on Reynolds number.

4. Further discussion

The mixing layer above the separation bubble entrains turbulent fluid which 'adds' turbulence and thereby imposes fluctuating strains on it. The velocity and length scales of the entrained fluid motion must be proportional to the velocity and length scales near attachment, and therefore in fixed proportion to the velocity and length scales of the bubble as a whole. However, it is to be expected that the effect of the fluctuating strain will depend upon Reynolds number when the latter is sufficiently low, because the mixing layer structures change significantly at low Reynolds number – as can be clearly seen in the flow visualizations of RF. Indeed, it was their flow visualization that led them in their choice of 'high' Reynolds number.

If the distance, x_o, required for the initial development of the mixing layer above the separation bubble is comparable to that of an isolated plane mixing layer then this development length is a significant fraction of the bubble length for the present Reynolds number range. Taking $X_A/h_f \sim 25$ and $x_o = 2000\theta_o$, and allowing for the splitter-plate thickness, then it follows that $x_o/X_A \approx 25(U_r h_f/\nu)^{-1/2}$. So, for $U_r h_f/\nu$ increasing from 1.6×10^3 to 1.6×10^4 the distance ratio x_o/X_A decreases from 0.6 to 0.2. As noted earlier in relation to figure 3, this range of x_o/X_A corresponds with the range over which the marked increase in $\overline{u^2}$ occurs, implying that the observed Reynolds-number dependence is a result of the structures of the early part of the mixing layer being less susceptible to fluctuating strain than later higher Reynolds number structures. The excellent flow visualization of Sutton, Devenport & Barkey Wolf (1990) shows the persistence of highly organized vortical structures at low Reynolds numbers. A smaller effect of fluctuating strain at low Reynolds numbers is also seen in a turbulent boundary layer beneath a turbulent free stream, where the increase in wall shear stress, for example, becomes progressively less as the momentum-thickness Reynolds number is decreased below about 2000 (Hancock & Bradshaw 1989; Blair 1983*a*, *b* and Castro 1984). Here, though, the fluid imposing the fluctuating rates of strain originates from near attachment, suggesting a feedback mechanism, dependent on Reynolds number, leading to a mixing layer having characteristics that are fundamentally different from an unperturbed layer.

Given the dependence on θ_o it is tempting to think that the development of the outer-layer part of the bubble would be more properly described in terms of x/θ_o

rather than x/X_A, in the early part of its development, and such a scaling does indeed show a tolerably good collapse of the measurements of $\overline{u^2}_{max}$ onto a single curve (Hancock 1994). However, a scaling based on x/θ_o alone, which leads to the single parameter $x/h_f(U_r h_f/\nu)^{1/2}$, overlooks the fact that the shear layer is intrinsically also a function of $U_r\theta_o/\nu$ or, equivalently, $U_r h_f/\nu$, and of the scales associated with the entrained turbulence.

As mentioned in the Introduction, it cannot be supposed that the other stresses remain in fixed proportion to $\overline{u^2}$ with change in Reynolds number. HM and CH give $\overline{v^2}$ and $\overline{w^2}$ as roughly equal to $0.7\overline{u^2}$, while $\overline{uv}$ is roughly $0.3\overline{u^2}$ for the lower Reynolds number measurements, and roughly $0.2\overline{u^2}$ for the higher. These latter factors imply that, over the present range, the shear stress increases only slightly with Reynolds number. Furthermore, the mean momentum balance given by CH (at $x/X_A = 0.7$) shows that the magnitude of $\partial\overline{u^2}/\partial x$ is roughly one-third the magnitude of $\partial\overline{uv}/\partial y$, which is roughly one-half of the magnitude of $\partial p/\partial x$. Therefore, the fairly small contribution from $\partial\overline{u^2}/\partial x$ and a comparatively small increase in the shear stress with Reynolds number would account for a comparatively small change in the mean flow. Clearly though, all four components of the Reynolds stress tensor need to be measured in one experiment.

5. Conclusions

The streamwise Reynolds stress $\overline{u^2}$ in the mixing layer above a two-dimensional separation bubble increases appreciably with Reynolds number even though there is little change in the mean flow, reconciling the substantial difference between the measurements of Ruderich & Fernholz (1986) and Castro & Haque (1987), and those of Hancock & McCluskey (1997) and Hancock & Castro (1993). The Reynolds stresses measured by Jaroch & Fernholz (1989) are incorrect and cannot be accounted for in terms of inadequate flow width or other identified source of error. Conversely, greater confidence can be attached to the measurements of Ruderich & Fernholz (1986), and also Castro & Haque (1987) (except near attachment), though it is clear that their near-wall flows were strongly influenced by end effects, and that the outer flow may not have been completely free of end effects. The present flow was about wide enough for end effects to have been insignificant.

The development length of an isolated mixing layer with initial conditions comparable to that of the overlying mixing layer is an appreciable proportion of the bubble length at low Reynolds numbers. It is argued that the dependence of the Reynolds stresses in the bulk of the flow is associated with the response of the early structures of the overlying layer to the fluctuating strain imposed on it by the recirculating flow, where the response at a low Reynolds number is less than it is at a high Reynolds number. The characteristics are therefore fundamentally different from an unperturbed layer, more so at a high Reynolds number. However, other parameters such as the reverse-flow factor shows no significant change, and the p.d.f. of the streamwise velocity fluctuations shows no noticeable change over and above the change in the fluctuation intensity. Drawing on other measurements, it is suggested that the change in $\overline{u^2}$ is larger than the changes in the other Reynolds stresses, accounting for the lack of change in the mean flow.

The surface shear stress and r.m.s. of the fluctuations, C_f and C_f', are also strongly Reynolds-number dependent, with C_f' varying in proportion to C_f. $\overline{u^2}$ in the outer part of the flow is not a scale for C_f'. The reverse flow factor, χ_{τ_w}, and the p.d.f. of the streamwise wall shear stress fluctuations do not change significantly, except in the

region of the secondary separation where χ_{τ_w} does change; χ_{τ_w} is close to 0.5 at both attachment and secondary separation locations, independent of Reynolds number. The reverse-flow factor for the velocity fluctuations, χ_u, and the normalized p.d.f. are also independent of Reynolds number, at least over the bulk of the bubble.

Most of the measurements presented here were made during two brief periods at the Hermann Föttinger Institut. Of the several people at HFI to whom I am very grateful for their friendship, assistance and encouragement, I wish to express particular thanks to Professor H. H. Fernholz for his invitation, and to Dr P. Dengel, M. Kalter, and Dr M. Schober. I am grateful too for the support and assistance given by my colleague, Professor I. P. Castro. Financial support was provided by Berlin University, DAAD and the British Council.

REFERENCES

Adams, E. W. & Johnston, J. P. 1988 Flow structure in the near-wall zone of a turbulent separated flow. *AIAA J.* **26**, 932–939.

Barkey Wolf, F. D. 1987 Swept and unswept separation bubbles. PhD thesis, University of Cambridge.

Blair, M. F. 1983*a* Influence of free-stream turbulence on turbulent boundary layer heat transfer and mean profile development, part 1 – experimental data. *J. Heat Transfer* **105**, 33–40.

Blair, M. F. 1983*b* Influence of free-stream turbulence on turbulent boundary layer heat transfer and mean profile development, part 2 – analysis of results. *J. Heat Transfer* **105**, 41–47.

Bradbury, L. J. S & Castro, I. P. 1971 A pulsed-wire technique for velocity measurements in highly turbulent flows. *J. Fluid Mech.* **49**, 657–691.

Bradshaw, P. & Wong, F. Y. F. 1972 The reattachment and relaxation of a turbulent shear layer. *J. Fluid Mech.* **52**, 113–135.

Castro, I. P. 1984 Effects of free-stream turbulence on low Reynolds number turbulent boundary layers. *Trans. ASME*: *J. Fluids Engng* **106**, 298–306.

Castro, I. P. & Cheun, B. S. 1982 The measurement of Reynolds stresses with a pulsed-wire anemometer. *J. Fluid Mech.* **118**, 41–58.

Castro, I. P., Dianat, M. & Bradbury, L. J. S. 1987 The pulsed-wire skin friction measurement technique. In *Turbulent Shear Flows 5*, pp. 278–290. Springer.

Castro, I. P. & Haque, A. 1987 The structure of a turbulent shear layer bounding a separation region. *J. Fluid Mech.* **179**, 439–468 (referred to herein as CH).

Cherry, N. J., Hillier, R. & Latour, M. E. M. P. 1984 Unsteady measurements in a separated and reattaching flow. *J. Fluid Mech.* **144**, 13–46.

Dengel, P., Fernholz, H. H. & Hess, M. 1986 Skin-friction measurements in two- and three-dimensional highly turbulent flows with separation. In *Advances in Turbulence* (ed. G. Compte-Bellot & J. Mathieu), pp. 470–479. Springer.

Devenport, W. J. & Sutton, E. P. 1991 Near-wall behaviour of separated and reattaching flows. *AIAA J.* **29**, 25–31.

Dianat, M. & Castro, I. P. 1989 Measurements in separating boundary layers. *AIAA J.* **27**, 719–724.

Eaton, J. K. & Johnston, J. P. 1981 A review of research on subsonic turbulent flow reattachment. *AIAA J.* **19**, 1093–1100.

Fernholz, H. H. 1994 Near-wall phenomena in turbulent separated flows. *Acta Mechanica* [*Suppl*] **4**, 57–67.

Hancock, P. E. 1994 Reynolds-number effects in separated flows. In *Advances in Turbulence V* (ed. V. R. Benzi), pp. 184–189. Kluwer.

Hancock, P. E. 1999 Measurements of mean and fluctuating wall shear stress beneath spanwise-invariant separation bubbles. *Exps. Fluids* **27**, 53–59.

Hancock, P. E. & Bradshaw, P. 1989 Structure of a boundary layer beneath a turbulent free stream. *J. Fluid Mech.* **205**, 45–76.

Hancock, P. E. & Castro, I. P. 1993 End effects in nominally two-dimensional separated flows. *Appl. Sci. Res.* **51**, 173–178 (referred to herein as HC).

Hancook, P. E. & McCluskey, F. M. 1997 Spanwise-invariant three-dimensional separated flow. *J. Exp. Thermal Fluid Sci.* **14**, 25–34 (referred to herein as HM).

Jaroch, M. 1985 Development and testing of pulsed-wire probes for measuring fluctuating quantities in highly turbulent flow. *Exps. Fluids* **3**, 315–322.

Jaroch, M. P. & Fernholz, H. H. 1989 The three-dimensional character of a nominally two-dimensional separated turbulent shear flow. *J. Fluid Mech.* **205**, 523–552 (referred to herein as JF).

Johnson, A. E. & Hancock, P. E. 1991 The effect of extra strain rates of streamline curvature and divergence on mixing layers. In *Turbulent Shear Flows 7* (ed. F. Durst *et al.*), pp. 253–267. Springer.

Jovic, S. & Driver, D. 1995 Reynolds number effect on the skin friction in separated flows behind a backward-facing step. *Exps. Fluids* **18**, 464–467.

Lasheras, J. C., Cho, J. S. & Maxworthy, T. 1986 On the origin and evolution of streamwise vortical structures in a plane, free shear layer. *J. Fluid Mech.* **172**, 231–258.

Le, H., Moin, P. & Kim, J. 1997 Direct numerical simulation of turbulent flow over a backward-facing step. *J. Fluid Mech.* **330**, 349–374.

Patel, V. C. 1965 Calibration of the Preston tube and limitations on its use in pressure gradients. *J. Fluid Mech.* **23**, 185–208.

Ruderich, R. & Fernholz, H. H. 1986 An experimental investigation of a turbulent shear flow with separation, reverse flow and reattachment. *J. Fluid Mech.* **163**, 283–322 (referred to herein as RF).

Smits, A. J. 1982 Scaling parameters for a time-average separation bubble. *Trans. ASME: J. Fluids Engng* **104**, 178–184.

Sutton, E. P., Devenport, W. J. & Barkey Wolf, F. D. 1990 Experimental studies of the reattachment of separated shear layers. *IUTAM Symp., Separated Flows and Jets*, (ed. V. V. Kozlov & A. V. Dovgal), pp. 573–588. Springer.

Townsend, A. A. 1976 *The Structure of Turbulent Shear Flow*. Cambridge University Press.